https://doi.org/10.1016/j.apenergy.2016.05.133

Study on an internally-cooled liquid desiccant dehumidifier with CFD model

Yimo Luo[1,*], Yi Chen[2], Hongxing Yang[2], Yuanhao Wang[1,*]

[1] Faculty of Science and Technology, Technological and Higher Education Institute of Hong Kong, Hong Kong

[2] Renewable Energy Research Group (RERG), Department of Building Services Engineering, The Hong Kong Polytechnic University, Hong Kong, China

*Corresponding author. Tel.: +852 2176 1887; Email address: yimo.luo@vtc.edu.hk (Y.M. Luo) or wangyuanhao@vtc.edu.hk (Y.H. Wang).

Abstract

The liquid desiccant air conditioning system is considered as a possible substitute of the traditional air conditioner mainly due to its characteristics of energy saving. The dehumidifier is a key component of the system therefore was chosen as the research object. It was found the present models conducted the simulation with lots of assumptions, especially ignoring the effect of flow behavior. Besides, most studies focused on the inlet and outlet parameter changes rather than the interior condition of the dehumidifier. To fill the research gap, a model for an adiabatic dehumidifier was established with CFD technology in authors' previous study. On the basis of it, a model was further developed in present work for internally-cooled liquid desiccant dehumidifier. The interior heat and mass transfer processes were then simulated with the model, followed by the detailed performance investigation. Analysis was conducted to investigate the influence of some factors, including inlet desiccant

temperature, desiccant flow rate and two types of internally cooling, and variable physical properties. The advantage of present study lied in its more in-depth analysis of interior condition of the dehumidifier. Besides, the study also demonstrated the necessity of considering the variable properties of desiccant solution during the simulation.

Keywords: Internally-cooled dehumidifier, CFD model

Nomenclature

A	contact area (m^2)
Ca	Capillary number (dimensionless)
Cp	specific heat at constant pressure ($J \cdot kg^{-1} \cdot K^{-1}$)
E	energy per unit mass ($J \cdot kg^{-1}$)
$\boldsymbol{F}$	source term in the momentum equation ($N \cdot m^{-3}$)
F_{ST}	source term due to surface tension ($N \cdot m^{-3}$)
$\boldsymbol{g}$	acceleration due to gravity ($m \cdot s^{-2}$)
h	sensible enthalpy ($J \cdot kg^{-1}$)
H_{lg}	latent heat of evaporation ($J \cdot kg^{-1}$)
H	heat flux ($W\ m^{-2}$)
J	mass flux ($kg \cdot m^{-3} \cdot s^{-1}$)
k	thermal conductivity ($W \cdot m^{-1} \cdot K^{-1}$),
K	local overall mass transfer coefficient ($kg \cdot m^{-2} \cdot s^{-1}$)
L	characteristic length (m)
m	the number of the species
n	the number of the phases
$\hat{n}$	the divergence of the unit normal
P	pressure (Pa)
Q	mass flow rate per unit length($kg \cdot m^{-1} \cdot s^{-1}$)
Re	Reynolds number (dimensionless)
S_E	source term in the energy equation ($W \cdot m^{-3}$)
S_{lg}	mass transfer source at the phase interface ($kg \cdot m^{-3}$)
S_C	heat exchange with cooling media ($W \cdot m^{-3}$)

t	time (s)
T	temperature (K)
$\boldsymbol{u}$, u	velocity vector ($\mathrm{m \cdot s^{-1}}$)
We	Weber number (dimensionless)
$W_{g,b}$, $W_{g,e}$	the humidity ratio of the bulk air and the equilibrium air humidity ratio to the desiccant solution ($\mathrm{kg \cdot kg^{-1}}$)
x , y	coordinate axis
$x_{k,q}$	mass fraction of the species k in the q^{th} phase

Greek characters

α	the volume fraction of phases
μ	dynamic viscosity ($\mathrm{kg \cdot m^{-1} \cdot s^{-1}}$)
ρ	density ($\mathrm{kg \cdot m^{-3}}$)
σ	surface tension coefficient ($\mathrm{N \cdot m^{-1}}$)
κ	curvature of free surface (dimensionless)
$\Gamma_{k,q}$	diffusion coefficient of the species k in the q^{th} phase ($\mathrm{m^2 \cdot s^{-1}}$)

Subscripts

a	air
eff	effective
g	gas phase
i, j	signal of coordinate axis
in	inlet
k	the k^{th} species
l	liquid phase
q	the q^{th} phase
s	solution
T	turbulence

w	wall

1. Introduction

The indoor environment has drawn increasing concerns as people spend most of their time in the buildings [1]. At present, the pleasant indoor environment still depends greatly on a large number of fossil fuels consumption, resulting energy crisis and serious environmental problems [2]. Therefore, it becomes more and more urgent to improve the energy utilization efficiencies [3-5] or resort to the utilization of renewable energy [6-8].

Studies show that there are mainly four factors which play great role in determining human comfort degree, i.e., temperature, relative humidity, pressure, air velocity [9]. According to ASHRAE standard 62-2001, the relative humidity needs to be kept in the range of 40% - 60% to meet the requirements of human comfort [10]. In the traditional air conditioner, the condensation dehumidification is employed for removing the excessive moisture from the air, and it takes up about 30 - 50% of the total energy consumption [11]. Then some liquid desiccants, such as lithium bromide (LiBr), lithium chloride (LiCl), calcium chloride ($CaCl_2$), were proposed for air dehumidification [12]. By introducing the liquid desiccant dehumidification into air conditioning, it is named the liquid desiccant air conditioning system, which can realize the separate control of temperature and humidity. Like the traditional air conditioner, the sensible heat of the air is removed by the cooling coil. However, the latent heat is controlled by removing the moisture from the air with liquid desiccant. As it needs not to reduce the air temperature to the dew-point temperature, the

evaporative temperature of the cooler is increased so as the cooler COP in the liquid desiccant air conditioning system is higher than that of the traditional air conditioner [13]. Therefore, compared with conventional vapor compression, a desiccant air conditioning system can save up to 40% energy [14, 15]. In addition, the dehumidification process is able to be driven by a relatively low regeneration temperature, i.e., between 60 and 75 °C. Thus, the low-grade thermal energy resources are capable of regeneration, such as geothermal energy, solar energy, and waste heat [16]. Moreover, it can avoid moisture condensation and reduce the wet surfaces which are the breeding ground for bacteria and mildew [17]. As a result, the liquid desiccant air conditioning system is considered as a possible substitute of the traditional air conditioner.

In the liquid desiccant air conditioning system, the dehumidifier is a key component, where the moist air is dehumidified. Lots of studies have been conducted to improve its performance by experiment [18, 19]. In terms of simulation, it was summarized three models had been developed for adiabatic dehumidifiers [20], i.e., finite difference model [21, 22], effectiveness NTU (ε-NTU) model [23] and some simplified solutions [24]. For the three different models, the finite difference model is used most often for its accuracy. However, it involves complicated iterative process, so it is only suitable for dehumidifier or regenerator design or operation optimization. Besides, some simplifications should be made to start the calculation. Compared with the finite difference model, two more assumptions are required for the $\varepsilon - NTU$ model.

Therefore, it is less accurate yet potential for saving computering time. In the simplified solutions, some more additive assumptions are made to be applicable for certain operation conditions. For example, the analytical solution of Ren at al. [52] is only suitable for the case where the solution flow rate and concentration change slightly as it assumed that the variation of the equilibrium humidity ratio of solution depended only on the change of the solution temperature. The complicated iteration could be avoided, so the simplified solutions have high efficiency of calculation. When it comes to internally-cooled dehumidifier, there are also three types of models developed on the basis of finite difference model [20]. They are models without considering liquid film thickness [25], models considering uniform liquid film thickness [26], and models considering variable liquid film thickness [27]. In the first model, the effect of velocity field on heat and mass transfer is ignored even though velocity, mass and energy are coupled. In the models considering uniform liquid film thickness, the film thickness and velocity field are kept unchanged in the process of calculation. It is found this model usually under-predict the dehumidification performance. The third model takes into consideration the influence of ever-changing velocity field, resulting in more accurate simulation. Based on the review, it is concluded that to simplify the heat and mass transfer process, lots of common assumptions had been made in present models, such as ignoring the influence of velocity, assuming the heat and mass transfer process to be steady state, and so forth. But it has been found the flow behaviors have strong effect on the performance of various heat and mass transfer devices and the process is unsteady [28, 29]. Thus, lots

of studies were conducted to investigate the gas-liquid flow characteristics. Moreover, most of the studies focused only on the inlet and outlet parameter changes rather than the interior condition of the dehumidifier. Besides, sometimes it regards the physical properties of liquid solution as constant during simulation.

In a heat and mass transfer equipment involving liquid flow, such as liquid desiccant dehumidifier, the liquid flow characteristics have great influence on their performance [35]. The varied film thickness is one of the important factors governing heat transfer [36]. It also has great impact on the mass transfer at the two phase interface [37]. Therefore, it is necessary to conduct dynamic analysis of the dehumidifier with considering the velocity field. On the other hand, lots of papers reported applying CFD (computational fluid dynamics) technology to describe the complex behaviors of the heat and mass transfer in the equipment [38, 39]. And CFD software Fluent is widely used as it is capable of simultaneous simulation of the fluid dynamics and mass transfer. Besides, it is convenient to obtain the dynamic results of treating process in the equipment interior. Therefore, Fluent is especially suitable for modeling the coupled flow, heat and mass transfer processes in the liquid desiccant dehumidifier. In the previous study, a model on the basis of Fluent had been established by the author to investigate the performance of adiabatic dehumidifiers under different conditions [35]. In the present paper, a two-dimensional CFD model was further developed for the internally-cooled dehumidifier with the following assumptions: 1) the flow, heat and mass transfer process occurs symmetrically in a channel; 2) there is

not heat and mass transfer in the third dimension; 3) the heat flux or the wall temperature is uniform. With the model, the interior heat and mass transfer process could be obtained. Analysis was conducted to investigate the influence of some factors, such as inlet desiccant temperature, desiccant flow rate, internally cooling, and variable physical properties.

2. Mathematical model

2.1 Geometric model

As shown in Fig. 1 [18], it is well known that the interior structure of liquid desiccant dehumidifiers is complicated, especially that of internally-cooled dehumidifiers. Considering the computing time, the structure was simplified to a group of vertical channels, one of which is presented in Fig. 2. The length of the channel was set to be 150 mm and the width 20 mm referring to the structured packing Mellapak 250Y. In a channel, the liquid flows down along the two walls and the moist air flows upward against the direction of the solution. In an ideal situation, it is completely symmetrical. To reduce the calculation load, only half of the channel was modeled in present study. In Fig. 2, the dotted line is the symmetric line of the channel. Unlike the adiabatic dehumidifier, some cold media was designed to flow behind the wall of the channel, removing the heat generated by dehumidification.

2.2 Governing equations

The basic governing equations include mass conservation equation, momentum

conservation equation, species transport equation, and energy conservation equation. In the paper, the VOF (Volume of Fraction) model was used to track the free surface of the two phase flow. Therefore, the properties of the substances in each computational cell were based on the volume fractions of the gas and liquid.

(1) Mass conservation equation

$$\frac{\partial}{\partial t}(\rho)+\nabla\cdot(\rho\boldsymbol{u})=0 \tag{1}$$

(2) Momentum conservation equation

$$\frac{\partial}{\partial t}(\rho\boldsymbol{u})+\nabla\cdot(\rho\boldsymbol{u}\boldsymbol{u})=-\nabla P+\nabla\cdot(\mu(\nabla\boldsymbol{u}+\nabla\boldsymbol{u}^{T}))+\rho\boldsymbol{g}+\boldsymbol{F} \tag{2}$$

In the above two equations, the properties ρ (density) and μ (viscosity) in each computational cell are represented by,

$$\rho=\alpha_{\mathrm{l}}\rho_{\mathrm{l}}+\alpha_{\mathrm{g}}\rho_{\mathrm{g}} \tag{3}$$

$$\mu=\alpha_{\mathrm{l}}\mu_{\mathrm{l}}+\alpha_{\mathrm{g}}\mu_{\mathrm{g}} \tag{4}$$

where α_{l}, ρ_{l} are the volume fraction and density of the liquid phase, α_{g} and ρ_{g} are the volume fraction and density of the gas phase.

To simulate the liquid film flow, it is necessary to consider the effect of the surface tension, especially when the liquid layer is very thin. Whether the surface tension has effect on the flow behavior can be judged by two non-dimensional numbers, which

are Re number and Ca number or Re number and We number. The following two equations show how to obtain Ca number and We number,

$$Ca = \frac{\mu u}{\sigma} \tag{5}$$

$$We = \frac{\rho L u^2}{\sigma} \tag{6}$$

When $\mathrm{Re} << 1$, Ca number is the main judgment standard. If $Ca >> 1$, the effect of surface tension can be ignored. When $\mathrm{Re} >> 1$, We number is the prominent factor. If $We >> 1$, the effect of surface tension can be ignored. In the paper, $\mathrm{Re} >> 1$, $We << 1$, thus the effect should be considered in the simulation. In the paper, the continuum surface tension (CSF) model proposed by Brackbill et al. [38] was utilized for covering the surface tension effect.

The surface tension at the two-phase surface is calculated by,

$$F_{\mathrm{ST}} = \sigma_{\mathrm{ij}} \frac{\rho \kappa_{\mathrm{i}} \nabla \alpha_{\mathrm{i}}}{(\rho_{\mathrm{i}} + \rho_{\mathrm{j}})/2} \tag{7}$$

where, σ is the surface tension coefficient, ρ is the volume-averaged density, κ is the free surface curvature defined in terms of the divergence of the unit normal $\hat{n}$ as,

$$\kappa = \nabla \cdot \hat{n} - \frac{1}{|n|}\left[\left(\frac{n}{|n|} \cdot \nabla\right)|n| - (\nabla \cdot n)\right] \tag{8}$$

where $\hat{n} = \frac{n}{|n|}$, $n = \nabla \alpha_q$

It is noted that the surface tension force F_{ST} in Eq. (7) was imposed on the momentum conservation equation (2) as a source term F .

(3) Species transport equation

$$\frac{\partial}{\partial t}\left(\alpha_q \rho_q x_{k,q}\right)+\nabla\cdot\left(\alpha_q \rho_q \boldsymbol{u} x_{k,q}-\alpha_q \Gamma_{k,q}\nabla x_{k,q}\right)=S_{lg,k} \tag{9}$$

q=1,.....,n k=1,.....,m

where $x_{k,q}$ is the mass fraction of the component k in the q^{th} phase. $S_{lg,k}$ represents the mass transfer source at the phase interface. $\Gamma_{k,q}$ is the diffusion coefficient.

In present paper, the mass transfer source $S_{lg,k}$ is the moisture absorbed from the humid air by the solution, and it is calculated by the equation below,

$$S_{lg,k} = K_g (W_{g,b} - W_{g,e}) A \tag{10}$$

where $W_{g,b}$ is the humidity ratio of the bulk air. $W_{g,e}$ is the equilibrium air humidity ratio to the desiccant solution. A is the contact area between the two phases. K_g is the overall mass transfer coefficient.

The mass transfer resistance at the interface is generally ignored [21], and the overall mass transfer coefficient can be calculated by [22],

$$\frac{1}{K_g}=\frac{1}{h_{m,g}}+\frac{1}{\psi h_{m,l}} \tag{11}$$

where ψ depends on the concentration and temperature of the bulk desiccant solution. For lithium chloride (LiCl) solution, it is obtained by the following equation,

$$\psi = a_0 + a_1 T_s + a_2 (T_s)^2 + a_3 (T_s)^3 \tag{12}$$

where

$$a_0 = -7.41610\times10^3 + 9.01270\times10^4 x_s - 3.97300\times10^5 x_s^{\,2} + 7.56527\times10^5 x_s^{\,3} - 5.20920\times10^5 x_s^{\,4}$$

$$a_1 = 1.98930\times10^3 - 2.42740\times10^4 x_s + 1.08917\times10^5 x_s^{\,2} - 2.13395\times10^5 x_s^{\,3} + 1.53709\times10^5 x_s^{\,4}$$

$$a_2 = -8.67870\times10^1 + 1.05970\times10^3 x_s - 4.76640\times10^3 x_s^{\,2} + 9.37240\times10^3 x_s^{\,3} - 6.78930\times10^3 x_s^{\,4}$$

$$a_3 = 0.97710 - 1.19300\times10^1 x_s + 5.36880\times10^1 x_s^{\,2} - 1.05670\times10^2 x_s^{\,3} + 7.66670\times10^1 x_s^{\,4}$$

Here, the local mass transfer coefficients $h_{m,g}$ and $h_{m,l}$ are calculated with the penetration model.

$$h_{m,g} = 2\sqrt{\frac{D_g}{\pi t_c}} \tag{13}$$

$$h_{m,l} = 2\sqrt{\frac{D_l}{\pi t_c}} \tag{14}$$

The contact time t_c is,

$$t_c = \frac{l}{u_{surf}} \tag{15}$$

where l is the liquid flow distance. u_{surf} is the surface velocity of the liquid film and it can be computed by,

$$u_{surf} = 1.5Q\left(\frac{3\mu Q}{\rho g}\right)^{-1/3} \tag{16}$$

(4) Energy conservation equation

$$\frac{\partial}{\partial t}(\rho E)+\nabla\cdot\left(\boldsymbol{u}(\rho E+P)\right)=\nabla\cdot\left[k_{\text{eff}}\nabla T-\sum h_{\text{k}}J_{\text{k}}\right]+S_{\text{E}} \tag{17}$$

The definition of the average energy E is as follows,

$$E=\frac{\sum_{q=1}^{n}\alpha_{\text{q}}\rho_{\text{q}}E_{\text{q}}}{\sum_{q=1}^{n}\alpha_{\text{q}}\rho_{\text{q}}} \tag{18}$$

where E_{q} is obtained according to the specific heat and the temperature of the q^{th} phase.

S_{E} is the energy source term. For the adiabatic dehumidification, the energy source is the latent heat generated by the mass transfer. As for the internally-cooled dehumidification, the heat exchange with the cooling media should also be considered, shown as follows,

$$S_{\text{E}}=\sum_{k=0}^{m-1}S_{\text{lg,k}}H_{\text{lg,k}}+S_{\text{C}} \tag{19}$$

where $H_{\text{lg,k}}$ is the enthalpy change of component k from phase gas to liquid or vice versa, and S_{C} is the heat exchange with the cooling media.

3. Solution strategies

A two-dimensional CFD model was developed for the internally-cooled dehumidifier with the following assumptions: 1) the flow, heat and mass transfer process occurs

symmetrically in a channel; 2) there is not heat and mass transfer in the third dimension; 3) the heat flux or the wall temperature is uniform. The software FLUENT was chosen for present simulation. The flow field was meshed by the structured grid. In authors' previous study [35], the grid independence had been checked. Four grids were meshed for the independence study, i.e., 49×250, 71×300, 71×500, and 81×500. The grid density increased gradually from the gas to the liquid phase as liquid film was much thinner than the air phase. In the x direction, the grid closed to the wall was set from 0.05 to 0.1 mm with the smallest size, and closed to the symmetry was from 0.2 to 0.3 mm with the largest size. In the y direction, a uniform grid was applied with sizes 0.6, 0.5 and 0.3 mm. The mass fraction of water vapor in the outlet air was monitored under the same inlet boundary conditions so as to judge the performance of the above four types of grids. Finally, it was found the grid 71×300 was best for simulation as a compromise of accuracy and computing efficiency.

The settings are introduced in the section. As mentioned above, VOF model was employed to track the free surface between the gas and liquid phase. The Semi-Implicit Method for Pressure Linked Equations (SIMPLE) was used to deal with pressure-velocity coupling. According to recommendation of Fluent 6.3 Users Guide, PRESTO! pressure interpolation scheme was adopted for pressure-velocity coupling equations. The second order upwind differencing was utilized to obtain more accurate and stable solutions for the transient formulation. As it requires time-accurate transient performance of VOF solution, the geometric reconstruction interpolation

scheme was used as the volume fraction discretization scheme.

The boundary conditions were set as follows. The liquid inlet was set as velocity inlet boundary, and the solution temperature and concentration could also be set by inputting values at the software interface. The liquid outlet was pressure outlet boundary. The gas inlet was pressure outlet boundary, and the air temperature and humidity were preset before the calculation. The gas outlet was velocity inlet boundary whose value was negative to induce reversed air flow. The wall was no-slip boundary shear condition. In the internally-cooled dehumidifier, the heat exchange would happen between the wall and cooling media. There were two cases, i.e., uniform temperature or heat flux density for the thermal boundary condition of the wall. Finally, the symmetry was set as symmetric boundary condition. A summary of boundary settings are marked on the physical model in Fig. 2.

Similar to previous simulation, lithium chloride (LiCl) was still selected as the desiccant. The reason is that in terms of inorganic desiccant, LiCl performs better than other common desiccant, i.e., lithium bromide (LiBr) and calcium dioxide ($CaCl_2$) [39]. The basic state of LiCl solution was set as follows: temperature 298 K, mass concentration 30%. Some important physical properties of LiCl solution at the basic point were presented in Table 1. It is well known that through dehumidification, both properties of moist air and desiccant solution would change. The properties include the density, thermal conductivity, mass diffusivity, viscosity, and so forth. FLUENT

contains all the physical properties of the moist air, which can be called during the calculation. For desiccant solution, the files of various properties of LiCl solution were written with programme C at different concentrations and temperatures. Then they were compiled to the software to be called.

4. Results and discussion

In authors' previous study [35], the validation of the CFD model had been conducted in terms of flow behavior and mass transfer condition. The results showed that the liquid film thickness obtained with present CFD model agreed well with that of Nusselt empirical formula, and the mass transfer amount also had acceptable difference from that calculated with the finite difference model. Therefore, CFD model was justified to be reliable to predict the performance of the dehumidifier. With the developed CFD model, the calculation was carried out under different conditions as shown in Table 2.

4.1 Influence of inlet desiccant temperature

It was found that the desiccant temperature had great impact on the dehumidification performance. As shown in Fig. 4, with the increase of desiccant temperature, the moisture concentration of outlet air increased sharply with a parabolical trend in general. One well-known reason was that the surface vapor pressure of the desiccant with higher temperature was higher accordingly. In addition, when the surface vapor pressure was higher, the driving force of moist absorption was reduced. In Fig. 5, it

was found when the temperature increased, the surface vapor pressure of the desiccant showed a similar parabolical increasing trend with that of moisture concentration of outlet air.

Another reason could be explained by Fig. 6. In Fig. 6, the interfacial velocities of solution under different inlet desiccant temperature were plotted. The results demonstrated that the increase of the inlet desiccant temperature would enhance the interfacial velocity of solution. The reason was the desiccant with higher temperature had lower viscosity. The above observation demonstrated that the high temperature desiccant worsened the dehumidification performance, not only by reducing the mass transfer driving force but also through decreasing the contact time between the desiccant and air.

In Fig. 4, the curve of the outlet air temperature under different inlet desiccant temperature was also plotted. The outlet air temperature increased almost linearly with the increase of inlet desiccant temperature. An increase of 1K of desiccant temperature would result in around 0.4K increase of outlet air temperature, so the effect was apparent. In Fig. 7, it showed the temperature distribution in the channel when the inlet desiccant temperature was 288K, 298K and 308K. The contours gave a clearer picture of the influence of the inlet desiccant temperature on the air temperature distribution. The color changed dramatically and it showed that the temperature of the air was affected significantly by the desiccant temperature due to the heat transfer.

In Fig. 4, by comparing the tendency of outlet air moisture concentration and outlet air temperature, it was speculated that the latent heat of phase change due to moist absorption played a relatively smaller role in determining the outlet air temperature for this channel. During the dehumidification, the air would be heated by two sources. One was the sensible heat transfer as a result of temperature difference with the desiccant. When the desiccant temperature increased, the sensible heat transfer would increase linearly, resulting in an almost linear increase of the outlet air temperature. Another one was the latent heat of phase change due to moist absorption. When the moisture absorption increased, the generated latent heat should increase accordingly, causing a similar increase trend of the outlet air temperature as well. In Fig. 4, it showed a parabolic increase of moisture concentration of outlet air. The larger the moisture concentration of out air was, the smaller the moisture absorption was, and the lower the latent heat was generated by absorption. Thus, it meant that with the increase of desiccant temperature, the produced latent heat of phase change should decrease in a parabolic trend, and the increment of outlet air temperature would decrease gradually. However, the curve of outlet air temperature was almost linear. Therefore, it was concluded that compared with the sensible heat source, the latent heat source had relatively smaller effect on the outlet air temperature. All of the above analysis demonstrated that the inlet desiccant temperature should be reduced as low as enough to achieve a good dehumidification performance.

Finally, the interfacial temperature along the liquid flow direction was also investigated in Fig. 8. It was observed that the change of the interfacial temperature was not discernible in the dehumidification process, which meant that the desiccant temperature changed a little as well. The reason was that the latent heat produced for absorption and the sensible heat due to the temperature difference were too small to heat the solution, as the heat capacity of the desiccant was big. On the other hand, the temperature of the moist air changed dramatically along the channel, whose temperature distribution had been shown in Fig. 7.

4.2 Influence of inlet solution flow rate

Under different inlet solution flow rate, the mass fraction of water vapor and temperature of outlet air had the similar variation trend. As shown in Fig. 9, it was observed that the initial increase of inlet solution flow rate would improve the dehumidification performance significantly while the effect reduced with further increase of inlet solution flow rate. It is well known that bigger solution flow rate will require larger pump power. Even though bigger solution flow rate is beneficial to dehumidification performance, it should trade-off between the dehumidification performance and pump power consumption.

By comparing the contours of temperature and mass fraction of water vapor in Fig. 10, a common point was found for each solution flow rate. It was found that the thermal diffusion was faster than the mass diffusion through observing the color change of

temperature and mass fraction of water vapor. It meant $Le > 1$ for all the cases. In early research, through comparing the simulation results with the experimental data of Fumo and Goswami [40], Babakhani [41] had pointed out that Le=1.1 instead of 1.0 was more preferable for the prediction of the performance of the dehumidifier. Thus, it could be verified that the present model possessed high accuracy.

4.3 Influence of internal cooling

In an internally cooled dehumidifier, besides the contact between air and desiccant, some cold source which can provide cool fluid like air or water is added to take away the latent heat produced in the process of dehumidification, which can be regarded as an isothermal process in general. As the latent heat is removed from the dehumidifier, it reduces the temperature rise of the solution and air, resulting in efficiency improvement. In this section, the dehumidification process with cooling was analyzed, including uniform heat-flux density condition and uniform wall temperature condition. The inlet status of solution and air were given as follows: solution temperature was 298K, solution concentration was 30.0%, air temperature was 303K, and mass fraction of water vapor in the moist air was 2.0%.

4.3.1. Uniform heat-flux density

In Fig. 11, the interface temperature along the flow direction under different heat fluxes was presented. Here the heat fluxes were set to be negative values to achieve cooling. It was observed that when the heat flux was lower, the interface temperature would

increase along the flow direction, resulting from the generation of latent heat in the dehumidification process. For present configuration, it could be read from Fig. 11 that the heat flux should be around 200 W m^{-2} to be isothermal dehumidification. In Fig. 11, it showed the interface temperature along the flow direction under different heat flux. The interface temperature was the solution temperature which was in contact with moist air. When the heat flux value was 200 W m^{-2}, the solution temperature kept almost unchanged along the flow direction. This process could be regarded as isothermal dehumidification. When the heat flux reached some value, not only the latent heat was removed, but also the temperature of the fluids in the channel was reduced.

As illustrated in Fig. 12, similar to interface temperature, the average temperature of outlet solution did not change too fast even through the minimum temperature of liquid film decreased sharply. As the channel of present model was too short, the cooling capacity was limited as well. Therefore, it seemed that the cooling did not contribute too much to the dehumidification performance by looking at Fig. 13. When the heat flux increased to 3000 W m^{-2}, the outlet air moisture content reduced by only 0.006% compared with that without cooling. However, by observing the tendency of Fig. 11, the interface temperature with cooling would be much lower than that without cooling if the channel was long enough, especially at the lower part of the channel. And it was well known that lower interface temperature meant stronger mass transfer driving force. Therefore, it is predicted from the trend that the effect of cooling would

be significant when the channel was long enough. As the computing time for long channel was unaffordable for the computer used in present study, another higher performance computer should be employed in further for more direct demonstration of the benefit of internal cooling with uniform heat flux density.

On the other hand, from Fig. 11, it was found that in the flow direction of the air, the interface temperature difference between the two cases (with cooling and without cooling) decreased gradually. The solution temperature with cooling would be lower than that without cooling, which was beneficial for dehumidification. The moisture content in the air without cooling would be larger than that with cooling. At the bottom part of the channel, the solution temperature was much lower with cooling than without cooling and the moisture content was equal for both cases, thus the driving force was higher with cooling than without cooling. At the upper part of the channel, the solution temperature was close for both cases and the moisture content was smaller with cooling than without cooling, therefore the driving force might be lower with cooling than without cooling. The above opposite effect might be another reason for the small influence of internal cooling. To sum up, a short channel can not reflect the advantage of uniform heat flux cooling, and it is critical to decide a suitable length of the channel for a counter-flow liquid desiccant dehumidifier with uniform heat flux cooling.

4.3.2. Uniform wall temperature

Keeping the wall at a certain temperature, the interface temperature along the flow direction was presented in Fig. 14. It was found 3K decrease of wall temperature would result in about 1K decrease of interface temperature at the outlet. When the wall temperature was the same with the inlet desiccant temperature, the temperature increase at the interface was so small to be ignored. The reason was the liquid film was very thin and the thermal conductivity coefficient of the solution was relatively large.

It was also observed that the interface temperature changed almost linearly along the solution flow direction for uniform wall temperature. Unlikely, for uniform heat-flux density case, the change rate of interface temperature was small initially and then increased gradually, approaching linear change. It demonstrated the overall heat transfer coefficient decreased along the flow direction with the constant heat-flux density. Therefore, it was concluded that the heat flux would be higher at the upper part than that at the lower part for uniform wall temperature case.

The influence of wall temperature on the dehumidification performance was illustrated in Fig. 15. Compared with the case of uniform heat-flux density, the influence was more obvious. The advantage of uniform wall temperature lied in its better control of interface temperature. As the overall heat transfer coefficient decreased along the flow direction, it would be more efficient to set higher heat-flux density at the upper part while lower at the lower part of the channel.

4.4 Influence of variable physical properties

It has been mentioned that in most of the previous studies, the properties of the desiccant solution were assumed constant, which is not the actual condition. In the present work, user defined files of various properties of LiCl solution were incorporated into the model, including the density, thermal conductivity, viscosity and so on. During the calculation, the properties of the solution would change simultaneously with the change of the temperature and concentration. In Fig. 16, the results for the cases of constant and variable properties are presented. It can be seen that the interfacial solution concentration was lower for variable properties case. Along the flow direction, the desiccant absorbed the moist air, resulting in the increase of the interfacial temperature and decrease of the concentration. As for the constant properties case, the properties of the solution did not change, the surface vapor pressure would keep constant through the process, which would be higher than the variable properties case. Therefore, the amount of moisture absorption would be higher in the constant properties case, resulting in the lower interfacial solution concentration. The study also demonstrated the necessity of considering the variable properties of the desiccant solution during the simulation.

5. Conclusions

In the present paper, a two-dimensional CFD model was developed for the internally-cooled dehumidifier with the following assumptions: 1) the flow, heat and

mass transfer process occurs symmetrically in a channel; 2) there is not heat and mass transfer in the third dimension; 3) the heat flux or the wall temperature is uniform. The dehumidifier performance was then investigated under different conditions. On the basis of calculation, several conclusions were summarized as follows,

1) With the increase of desiccant temperature, the moisture concentration of outlet air increased sharply with a parabolical trend and the outlet air temperature increased almost linearly. An increase of 1K of desiccant temperature would result in around 0.4K increase of outlet air temperature.
2) It was concluded that in the dehumidification process, compared with the sensible heat transfer between desiccant and air, the latent heat generated by moist absorption had relatively smaller effect on the outlet air temperature.
3) By observing the velocity field, it was found that high temperature desiccant worsened the dehumidification performance, not only by reducing the mass transfer driving force but also through decreasing the contact time between the desiccant and air.
4) The initial increase of inlet solution flow rate would achieve significant improvement of dehumidification performance while the effect reduced with further increase of inlet solution flow rate. Thus, it should trade-off between the dehumidification performance and desiccant pump power consumption.
5) By looking into the contours of temperature and mass fraction of water vapor under different inlet solution flow rate, it was found that $Le > 1$ for the present simulation. The results showed good agreement with the previous experimental

study.

6) The heat flux density should be around 200 W m^{-2} to be isothermal dehumidification for present configuration.
7) A short channel can not reflect the advantage of uniform heat flux cooling, and it is critical to decide a suitable length of the channel for a counter-flow liquid desiccant dehumidifier with uniform heat flux cooling.
8) For countercurrent flow dehumidifier, it would be more efficient to set higher heat-flux density at the upper part while lower at the lower part of the channel.
9) The study also demonstrated the necessity of considering the variable properties of desiccant solution during the simulation.

Finally, in this paper, the dehumidification process with cooling was analyzed, including uniform heat-flux density condition and uniform wall temperature condition. Except for them, it is possible to set other internal cooled boundaries in FLUNET by incorporating the user defined files. Further studies are required for investigating the influence of more other cooling conditions.

Acknowledgement

The work described in this paper was supported by the Hong Kong Polytechnic University Research Institute for Sustainable Urban Development (RISUD) and Shenzhen Peacock Plan (KQTD2015071616442225).

Reference

[1] Luo YM, Wang M, Yang HX, Lu L, Peng JQ. Experimental study of internally cooled liquid desiccant dehumidification: application in Hong Kong and intensive analysis of influencing factors. Build Environ 2015;93:210-20.

[2] Majoumerd MM, Raas H, De S, Assadi M. Estimation of performance variation of future generation IGCC with coal quality and gasification process -Simulation results of EU H2-IGCC project. Appl Energy 2014;113:452-62.

[3] Yan J, Chou SK, Desideri U, Tu ST, Jin HG. Research, development and innovations for sustainable future energy systems. Appl Energy 2013;112:393-5.

[4] Fan HM, Shao SQ, Tian CQ. Performance investigation on a multi-unit heat pump for simultaneous temperature and humidity control. Appl Energy 2014,113:883-890.

[5] She XH, Yin YG, Zhang XS. Suggested solution concentration for an energy-efficient refrigeration system combined with condensation heat-driven liquid desiccant cycle. Renew Energ 2015;83:553-64.

[6] Yu Y, Sun DM, Wu K, X Y, Chen HJ, Zhang XJ, Qiu LM. CFD study on mean flow engine for wind power exploitation. Energ Convers Manage 2011;52:2355-9.

[7] Li QA, Maeda T, Kamada Y, Murata J, Furukawa K, Yamamoto M. Effect of number of blades on aerodynamic forces on a straight-bladed Vertical Axis Wind Turbine. Energy 2015;90:784-95.

[8] Li QA, Maeda T, Kamada Y, Murata J, Yamamoto M, Ogasawara T, Shimizu K, Kogaki T. Study on power performance for straight-bladed vertical axis wind turbine by field and wind tunnel test Renew Energ 2016;90:291-300.

[9] Qian MF, Ye M. A method in evaluating the pleasantness of weather for tourist. Journal of Chengdu Institute of Meteorology 1996;3:128-34.

[10] ASHRAE. ASHRAE standard 62-2001: Ventilation for acceptable indoor air quality. ASHRAE, Atlanta, 2001.

[11] Li Z, Jiang Y, Liu XH, Qu KY. Energy efficiency of dehumidification process from buildings. HVAC&R Res 2005;35(1):90-6.

[12] Luo YM, Shao SQ, Xu HB, Tian CQ. Dehumidification performance of [EMIM]BF_4. Appl Therm Eng 2011;31:2772-7.

[13] She XH, Yin YG, Zhang XS. Thermodynamic analysis of a novel energy-efficient refrigeration system subcooled by liquid desiccant dehumidification and evaporation. Energ Convers Manage 2014;78:286-96.

[14] Potnis SV, Lenz TG. Dimensionless Mass-Transfer Correlations for Packed-Bed Liquid Desiccant Contactors. Ind Eng Chem Res 1996;35 (11): 4185-93.

[15] Oberg V, Goswami DY. Advances in solar energy: an annual review of research and development. American Solar Energy Society Inc 1998;12:431-70.

[16] Xie XY, Jiang Y, Tang YD, Yi XQ, Liu SQ. Simulation and experimental analysis of a fresh air-handling unit with liquid desiccant sensible and latent heat recovery. Build Simul 2008;1:53-63.

[17] Luo YM, Yang HX, Lu L. Dynamic and microscopic simulation of the counter-current flow in a liquid desiccant dehumidifier. Appl Energy 2014;136: 1018-25.

[18] Luo YM, Shao SQ, Xu HB, Tian CQ, Yang HX. Experimental and theoretical

research of a fin-tube type internally-cooled liquid desiccant dehumidifier. Appl Energy 2014;133:127-34.

[19] Luo YM, Wang M, Yang HX, Lu L, Peng JQ. Experimental study of falling film thickness in a dehumidifier of liquid desiccant air conditioning system. Energy 2015;84:239-46.

[20] Luo YM, Yang HX, Lu L, Qi RH. A review of the mathematical models for predicting the heat and mass transfer process in the liquid desiccant dehumidifier. Renew Sust Energ Rew 2014;31:587-99.

[21] Luo YM, Shao SQ, Xu HB, Tian CQ. Dehumidification performance of [EMIM]BF_4. Appl Therm Eng 2011;31(14-15):2772-77.

[22] Luo YM, Shao SQ, Qin F, Tian CQ, Yang HX. Investigation of feasibility of ionic liquids used in solar liquid desiccant air conditioning system. Sol Energy 2012;86:2718-24.

[23] Ren CQ. Corrections to the simple effectiveness-NTU method for counterflow cooling towers and packed bed liquid desiccant–air contact systems. Int J Heat Mass Transfer 2008;51:237-45.

[24] Khan AY, Ball HD. Development of a generalized model for performance evaluation of packed-type liquid sorbent dehumidifiers and regenerators. ASHRAE Transactions 1992;98:525-33.

[52] Ren CQ, Jiang Y, Zhang YP. Simplified analysis of coupled heat and mass transfer processes in packed bed liquid desiccant-air contact system. Sol Energy 2006;80(1):121-31.

[25] Zhang T, Liu XH, Jiang JJ, Chang XM, Jiang Y. Experimental analysis of an internally-cooled liquid desiccant dehumidifier. Build Environ 2013;60:1-10.

[26] Ali A, Vafai K, Khaled ARA. Analysis of heat and mass transfer between air and falling film in a cross flow configuration. Int J Heat Mass Transfer 2004;47:743-55.

[27] Diaz G. Numerical investigation of transient heat and mass transfer in a parallel-flow liquid-desiccant absorber. Heat Mass Transfer 2010;46:1335-44.

[28] Song MJ, Pan DM, Li N, Deng SM. An experimental study on the negative effects of downwards flow of the melted frost over a multi-circuit outdoor coil in an air source heat pump during reverse cycle defrosting. Appl Energy 2015;138:598-604.

[29] Song MJ, Deng SM, Pan DM, Mao N. An experimental study on the effects of downwards flowing of melted frost over a vertical multi-circuit outdoor coil in an air source heat pump on defrosting performance during reverse cycle defrosting. Appl Therm Eng 2014;67(1-2):258-65.

[35] Luo YM, Yang HX, Lu L. Liquid desiccant dehumidifier: development of a new performance predication model based on CFD. Int J Heat Mass Transfer 2014;69:408-16.

[36] Chun MH, Kim KT. Assessment of the new and existing correlations for laminar and turbulent film condensations on a vertical surface. Int Commun Heat Mass 1990;17:431-41.

[37] Himmelblau DM. Diffusion of dissolved gases in liquid. Chem Rev 1964;64:527-50.

[38] Arpino F, Cortellessa G, Mauro A. Transient thermal analysis of natural

convection in porous and partially porous cavities. Numerical Heat Transfer, Part A 2015;67:605-31.

[39] Arpino F, Cortellessa G, Dell'lsola M, Massarotti N, Mauro A. High order explicit solutions for the transient natural convection of incompressible fluids in tall cavities. Numerical Heat Transfer, Part A 2014;66:839-62.

[38] Babakhani D. Developing an application analytical solution of adiabatic heat and mass transfer processes in a liquid desiccant dehumidifier/regenerator. Chem Eng Technol 2009;32(12):1875-84.

[39] I.P. Koronaki, R.I. Christodoulaki, V.D. Papaefthimiou, E.D. Rogdakis, Thermodynamic analysis of a counter flow adiabatic dehumidifier with different liquid desiccant materials, Appl. Therm. Eng. 50 (2013) 361-373.

[40] Brackbill JU, Kothe PB, Zemach C. A continuum method for modeling surface tension. J Comput Phys 1992;100:335-54.

[41] Fumo N, Goswami DY. Study of an aqueous lithium chloride desiccant system: air dehumidification and desiccant regeneration. Sol Energy 2002;62(4):351-61.

[21] Bird RB, Stewart WE, Lightfoot EN. Transport Phenomena. Wiley, New York, 1960.

[22] Zhang L, Hihara E, Massuoka F, Dang CB. Experimental analysis of mass transfer in adiabatic structured packing dehumidifier/regenerator with liquid desiccant. Int J Heat and Mass Tran 2010;53:2856-63.

Fig. 1. The fin-tube type internally-cooled liquid desiccant dehumidifier [18]

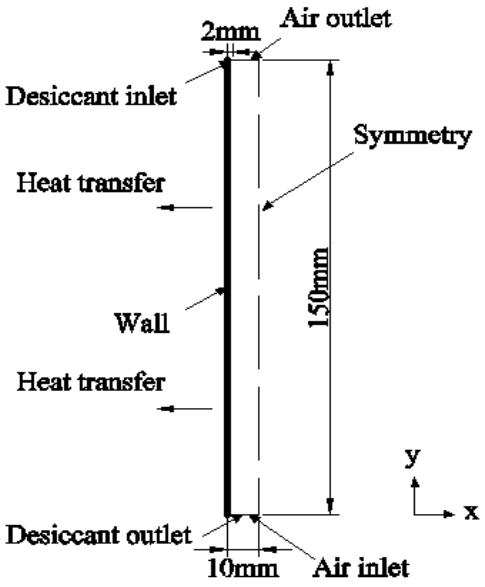

Fig. 2. Simplified physical model of an internally-cooled dehumidifier

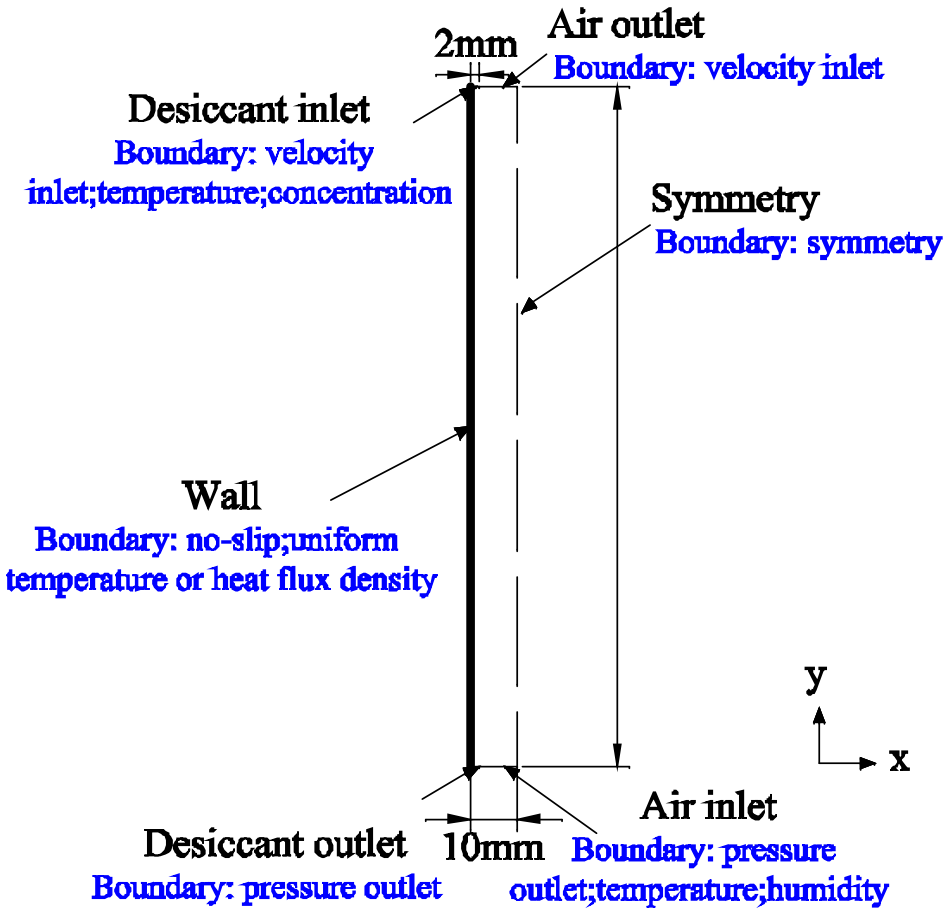

Fig. 3. Simplified physical model of an internally-cooled dehumidifier and boundary settings

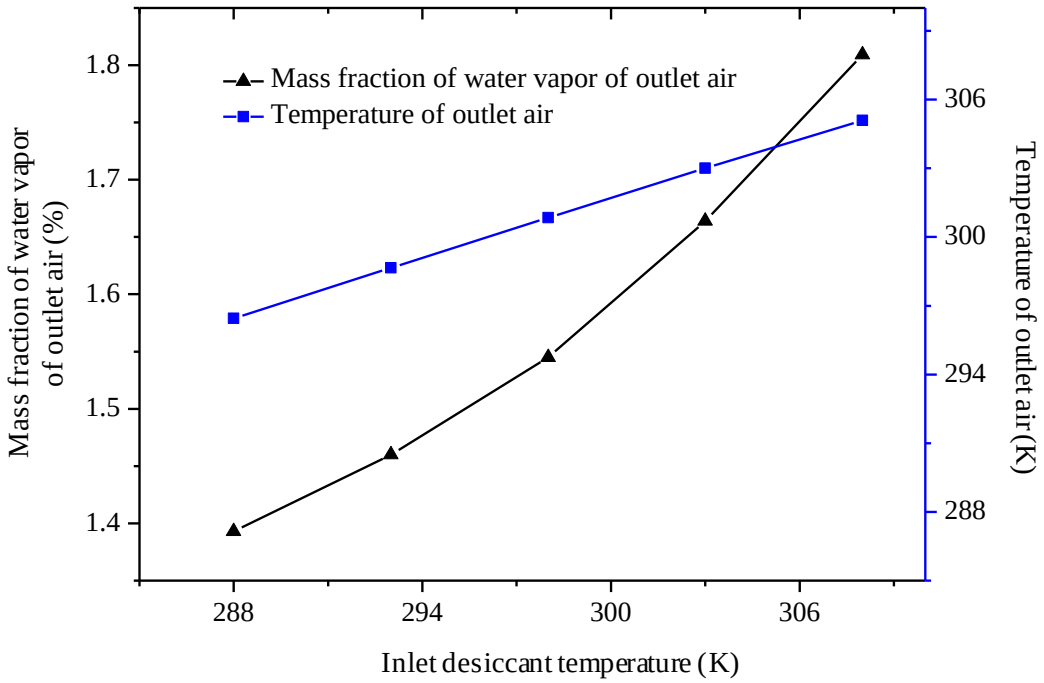

Fig. 4. Mass fraction of water vapor and temperature of outlet air under different inlet desiccant temperature

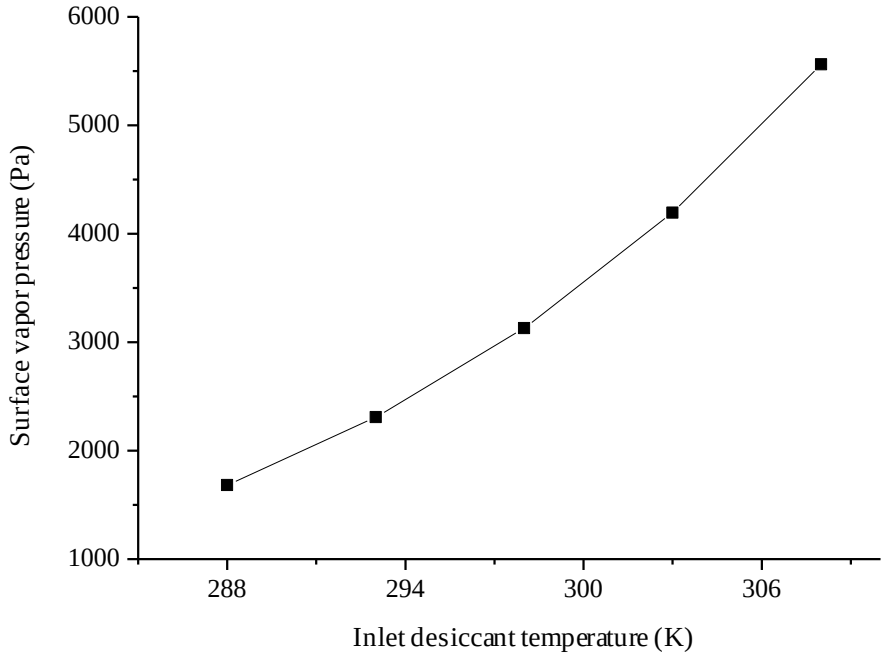

Fig. 5. Surface vapor pressure of desiccant solution under different inlet desiccant temperature

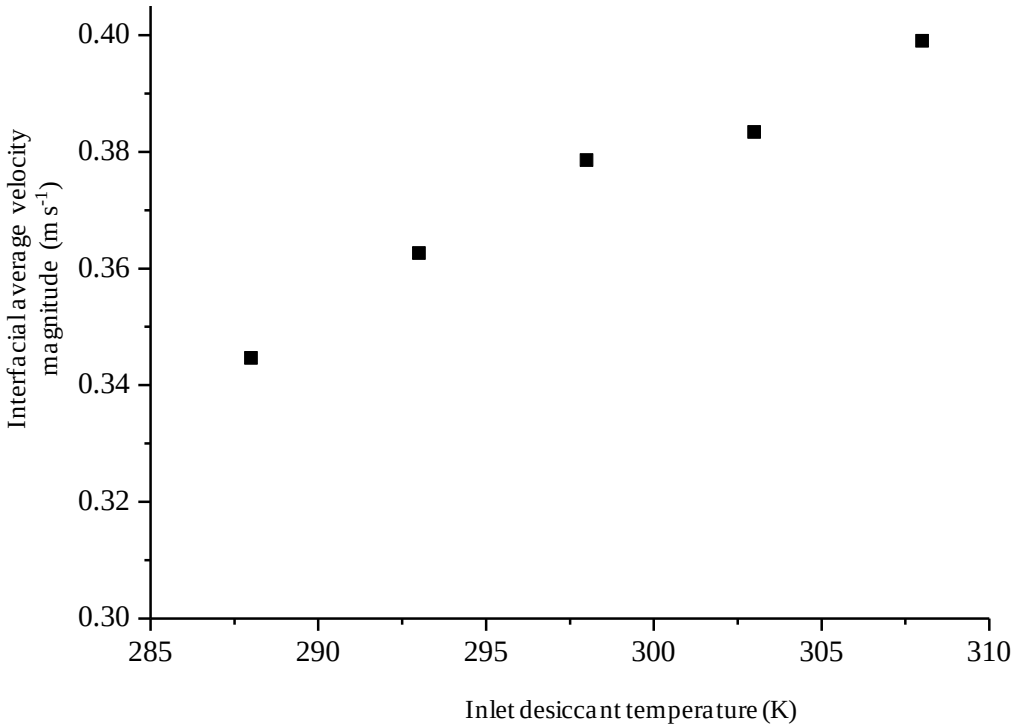

Fig. 6. Interfacial average velocity magnitudes under different inlet desiccant temperature

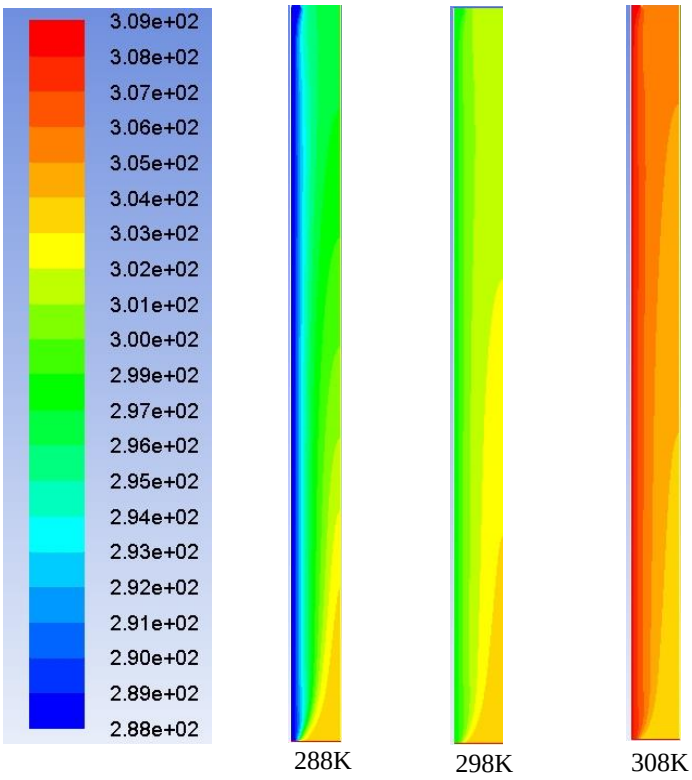

Fig. 7. Contour of temperature under different inlet desiccant temperature (K)

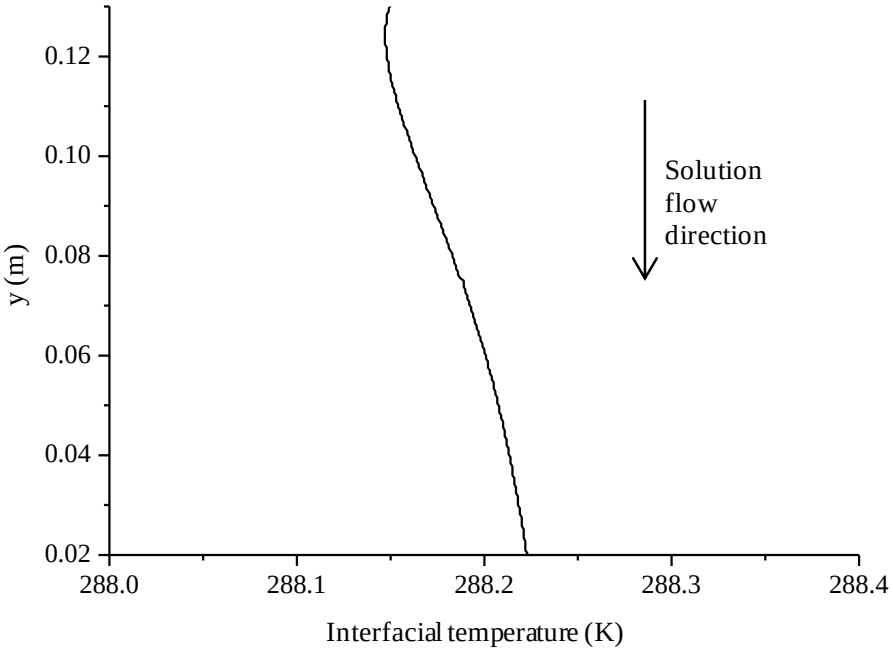

Fig. 8. Interfacial temperature along the liquid flow direction

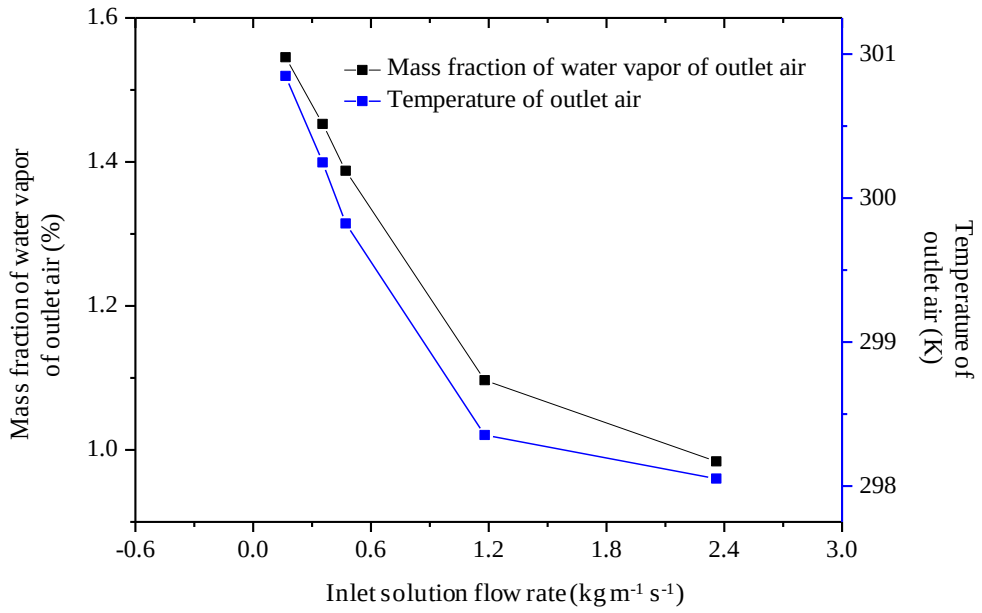

Fig. 9. Mass fraction of water vapor and temperature of outlet air under different inlet solution flow rate

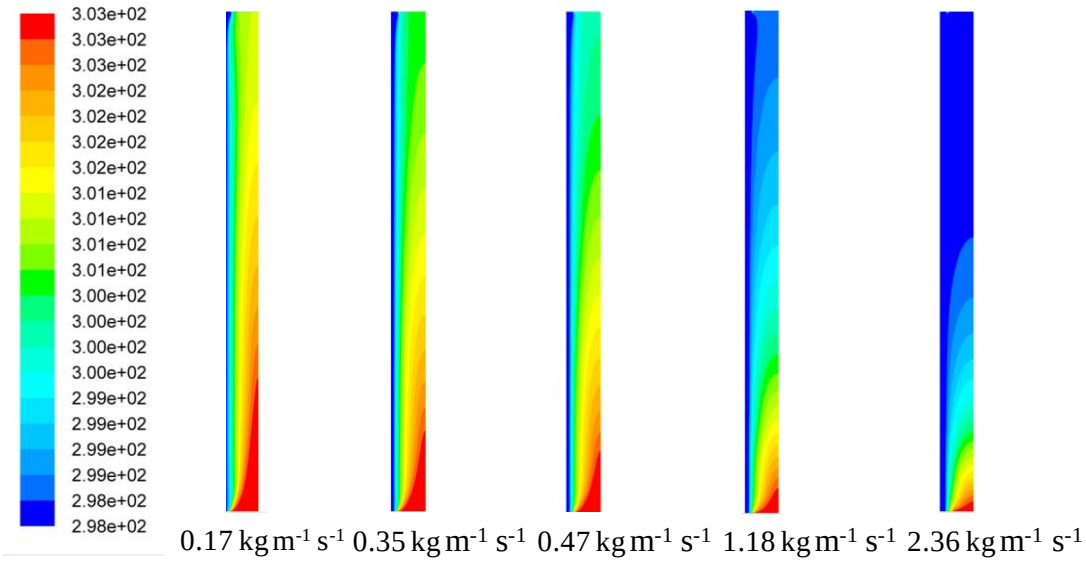

(a) Contours of temperature (K)

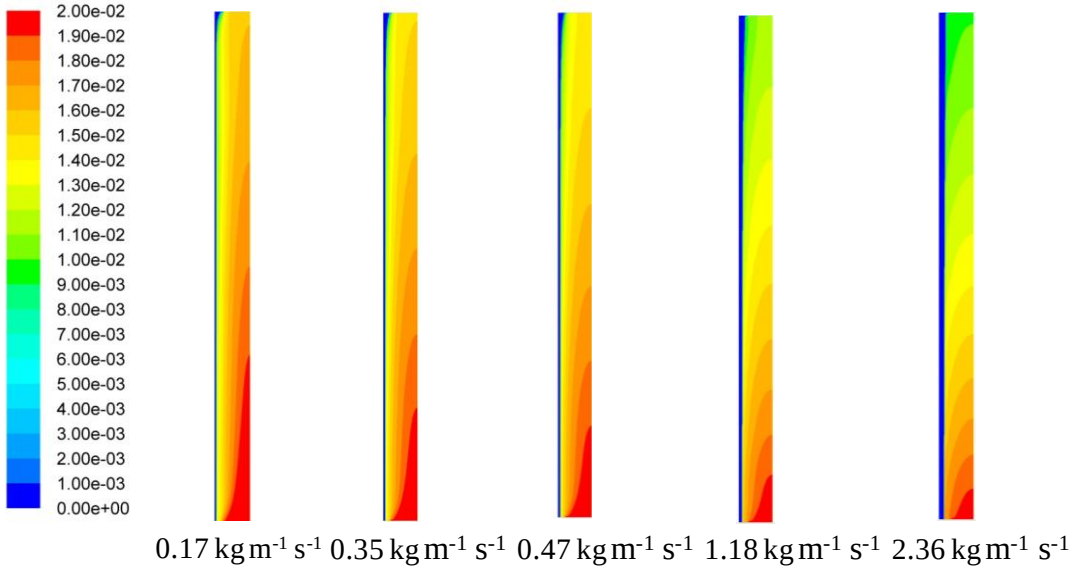

(b) Contours of mass fraction of water vapor

Fig. 10. Contours of temperature and mass fraction of water vapor under different solution flow rate

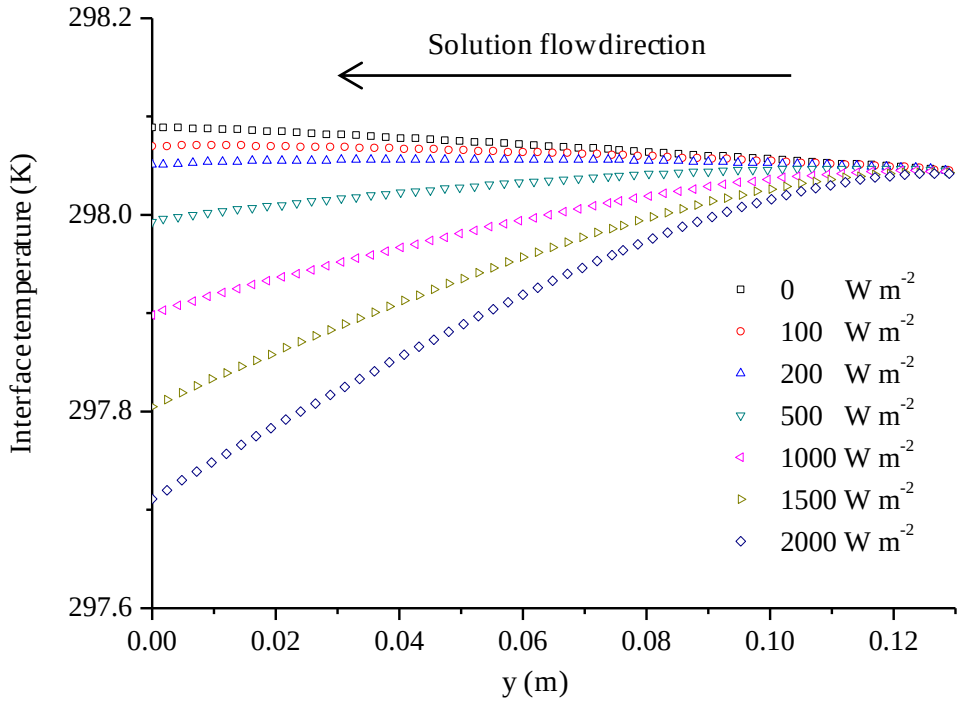

Fig.11. Interface temperature along the flow direction under different heat flux

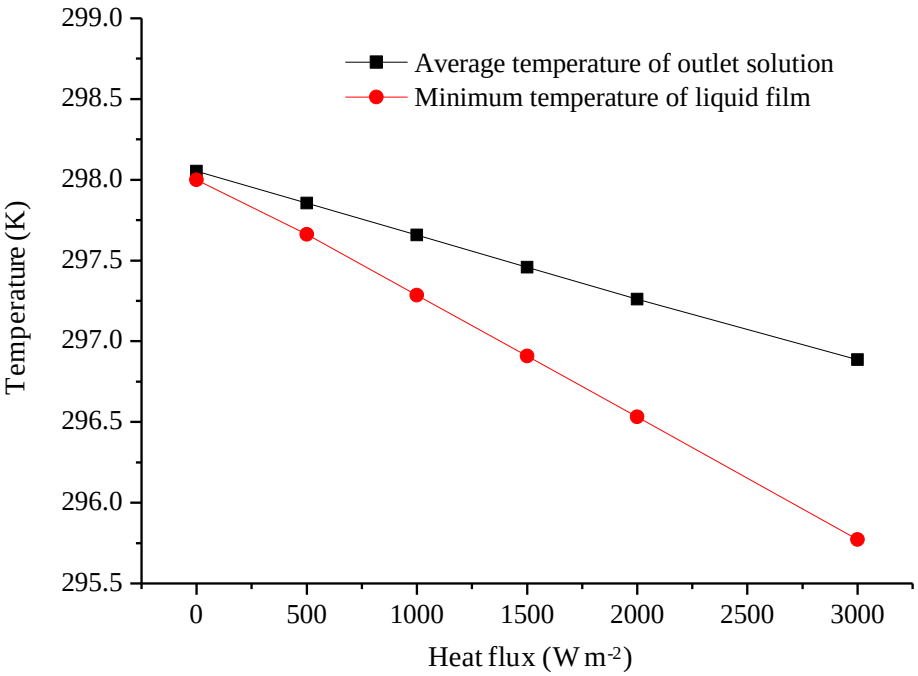

Fig. 12. Temperature of liquid phase under different heat flux

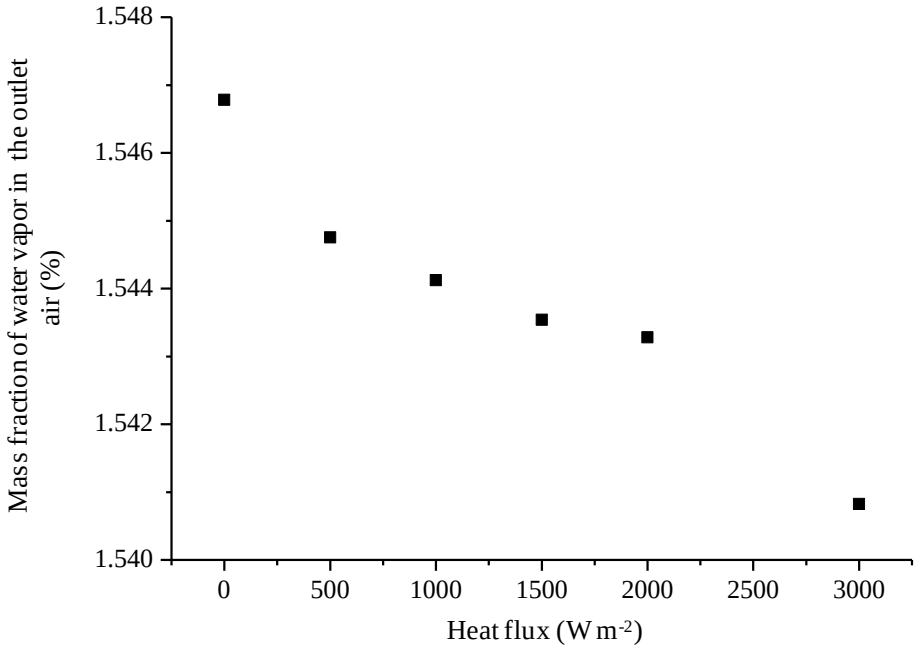

Fig. 13. Water content in the outlet air under different heat flux

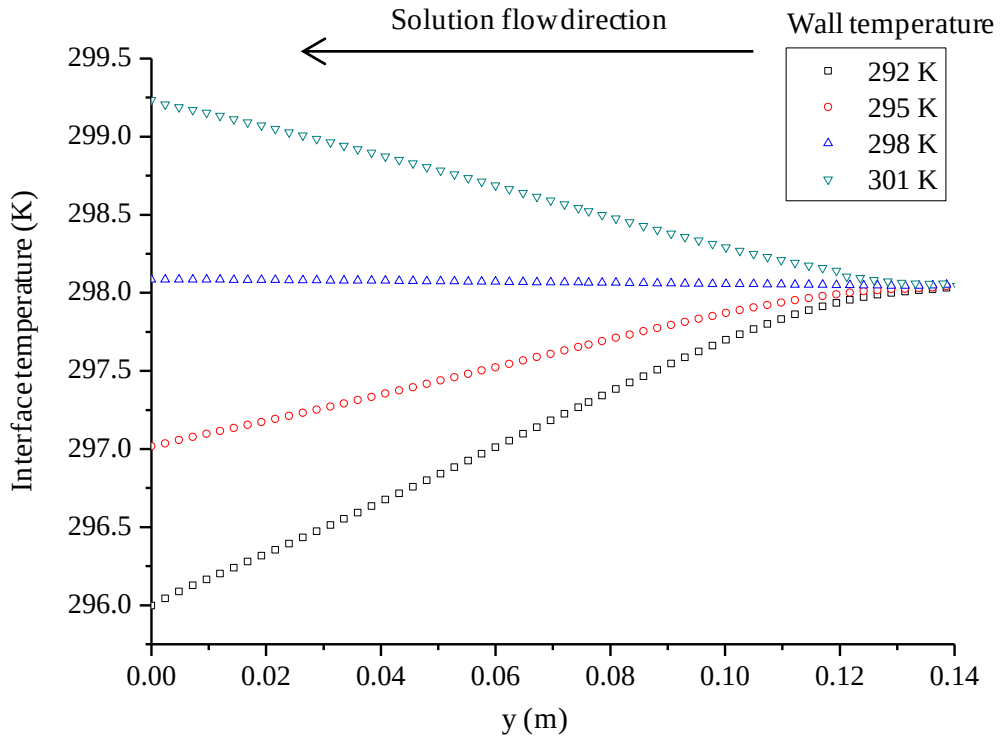

Fig. 14. Interface temperature along the flow direction under different wall temperature

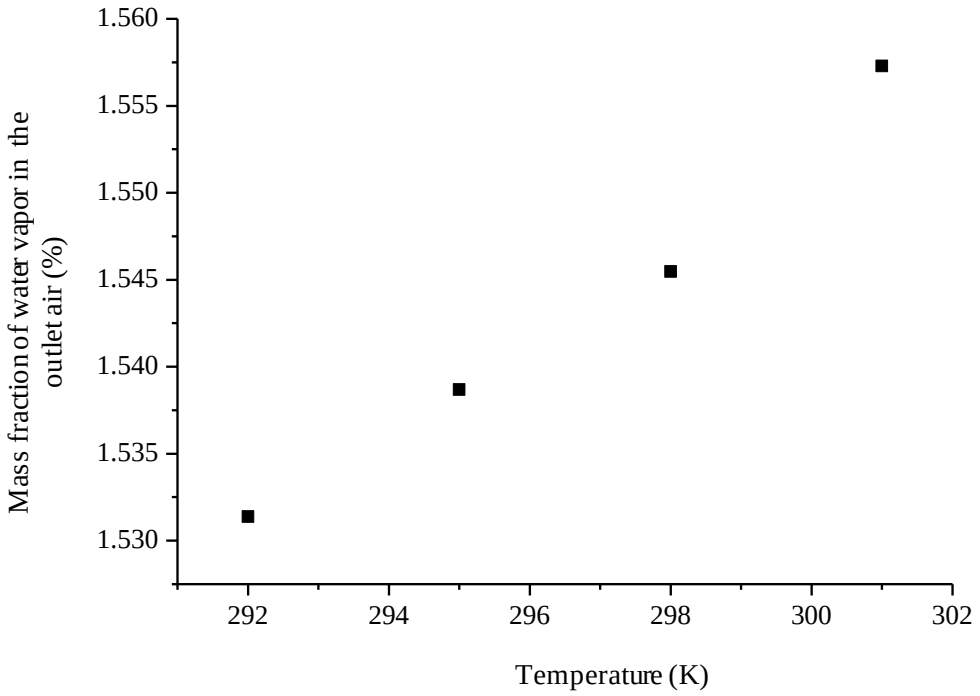

Fig. 15. Water content in the outlet air under different wall temperature

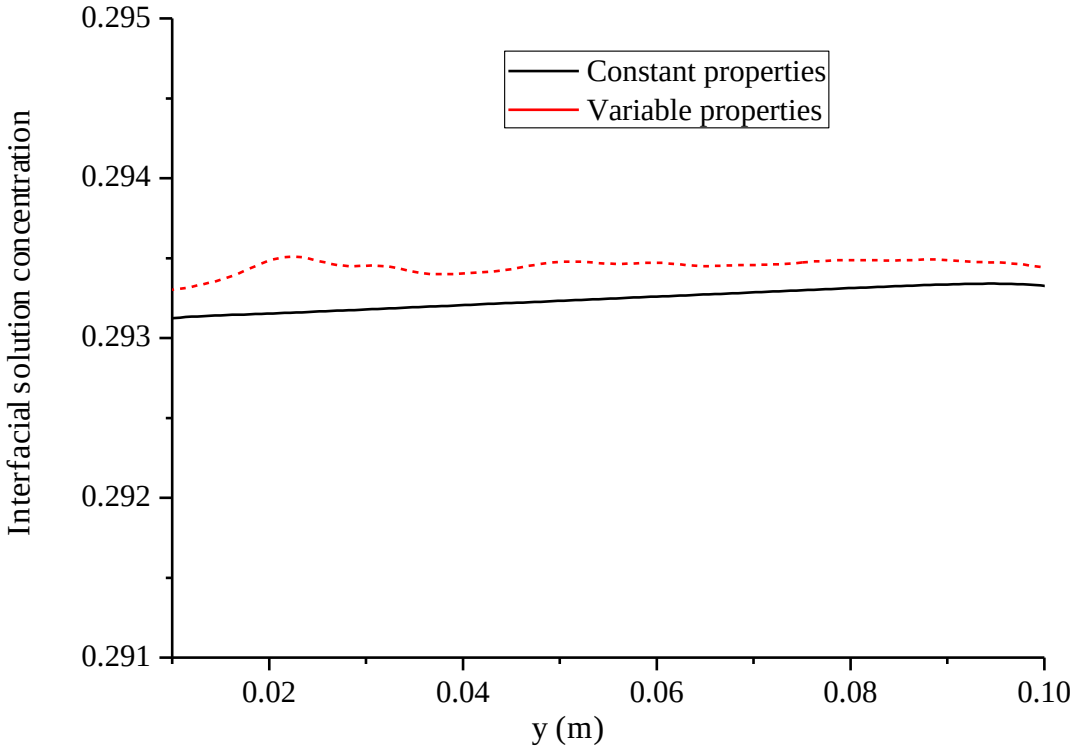

Fig. 16. The profile of interfacial solution concentration along the film flow